Journal Pre-proof

Zeolites in acid vitreous rocks, southern Mendoza, Argentina

Francisco Locati, Fernanda Cravero, Silvina Marfil, Leticia Lescano, Lenís Madsen, Pedro Maiza

PII: S0895-9811(19)30448-1

DOI: https://doi.org/10.1016/j.jsames.2019.102440

Reference: SAMES 102440

To appear in: *Journal of South American Earth Sciences*

Received Date: 26 August 2019

Revised Date: 20 November 2019

Accepted Date: 22 November 2019

Please cite this article as: Locati, F., Cravero, F., Marfil, S., Lescano, L., Madsen, Leni., Maiza, P., Zeolites in acid vitreous rocks, southern Mendoza, Argentina, *Journal of South American Earth Sciences* (2019), doi: https://doi.org/10.1016/j.jsames.2019.102440.

Zeolites in acid vitreous rocks, southern Mendoza, Argentina

Francisco Locati[a*] , Fernanda Cravero[b], Silvina Marfil[c], Leticia Lescano[c], Lenís Madsen[c] and Pedro Maiza[c]

[a*] *CICTERRA (CONICET-UNC). Av. Vélez Sarsfield 1611, Córdoba (X5016GCA), Argentina. flocati@unc.edu.ar*

[b] *CETMIC, CONICET-CIC, Centenario Av. and 506, Gonnet (B1897), La Plata, Argentina. fcravero@cetmic.unlp.edu.ar*

[3] *Geology Department. Universidad Nacional del Sur. CGAMA - CIC. San Juan 670, Bahía Blanca (B8000), Argentina. smarfil@uns.edu.ar, leticia.lescano@uns.edu.ar, lenismad@gmail.com, pmaiza@uns.edu.ar*

ABSTRACT

A mordenite-rich deposit located in the south of the province of Mendoza (Argentina) was studied. The host rock in this area has not been previously described and corresponds to rhyolitic lavas of high-K calc-alkaline series. Petrographic, mineralogical and geochemical analyses of fresh and altered rocks are shown, and a proposal for the alteration process and the stratigraphic position of the protolith is presented. The main mordenite-rich sectors developed in zones of autobreccias of high permeability, with minor clinoptilolite, smectites, secondary K-feldspars, and colloform silica. The proportion of relict glass vs. alteration minerals is variable and mainly depends on the texture (permeability) of the host rock. The studied rhyolites overlie the Upper Cretaceous sediments of the Neuquén Group

and are covered by Tertiary basalts of the Molle Eruptive Cycle and Quaternary sediments. Geochemically, they present similarities with rhyolitic rocks of Cordón del Burrero Volcanic Complex of Lower to Middle Miocene age.

Keywords: rhyolite, mordenite, clinoptilolite, beidellite-montmorillonite

1. INTRODUCTION

Zeolites occur in different geological environments in Argentina (mainly diagenetic or hydrothermal), but only in the province of La Rioja a clinoptilolite-rich zeolitized tuff is commercially exploited (Gargiulo *et al*., 2017). A very interesting mordenite-rich prospect was found associated with glassy rocks in southern Mendoza, Argentina. Bengochea *et al.* *(*1997) performed some preliminary mineralogical studies on the outcrop. However, there have not been additional studies that might contribute to the development of the deposit for its exploitation.

Zeolite minerals have been recognized as major constituents of altered volcaniclastic rocks in various geological environments, such as burial metamorphism, saline alkaline lakes, marine and fresh waters, geothermal fields, etc. (Marantos *et al*., 2012 and references therein). Clinoptilolite and mordenite as the main product of alteration are widely distributed in nature. They have been found as diagenetic minerals formed from glassy rhyolitic fragments such as pumices, scorias, shards, and vitric ash (Ghiara *et al*., 1999; Cappelletti *et al*., 2001; Mormone *et al*., 2018), as the result of hydrothermal processes on vitric tuffs and perlites (Demina *et al*., 2015) and on pyroclastic/volcaniclastic material

(Phillips, 1983; Sheppard *et al*., 1988; Tsolis-Katagas and Katagas, 1990; Kitsopoulos, 1997).

The objective of the present work is to determine the origin of the alteration and the formation process of the zeolites occurring south of Malargüe (province of Mendoza), and to study the associated minerals evaluating the mobility of major, minor, and trace elements during the alteration process. The stratigraphic position of the protolith will also be established, in order to help understand the origin of fluids that could have participated in the alteration process.

2. MATERIALS AND METHODS

The study area is located in the province of Mendoza (Argentina), 120 km south of Malargüe, near La Pasarela bridge on No. 40 National Route (Fig. 1). The alteration zone was delimited in the field by discontinuous outcrops of zeolitized vitreous rocks. Different units were sampled to establish the lithological and structural control that defines the distribution and variation of the alteration.

A total of 47 samples of the fresh and altered vitreous rocks were collected. First, all samples were studied by petrography and complemented by X-ray diffraction (XRD) analysis. Petrographic determinations on thin sections were made with an Olympus B2-UMA trinocular petrographic microscope, and photomicrographs were taken with parallel and crossed nicols (//N, XN). Mineral abbreviations according to Whitney and Evans (2010) were used. XRD analyses were performed using a PANalytical X'Pert PRO diffractometer, with Cu $K\alpha_{1,2}$ radiation (λ = 1.541840 Å) filtered with a graphite monochromator in the diffracted beam, operating at 40 kV and 40 mA. XRD patterns were

recorded on whole rock (powder) from 4 to 60º 2θ with increments of 0.02° 2θ and a counting time of 14 s per step.

Morphological characterization of the main alteration phases was performed on secondary electron (SE) images obtained by a LEO EVO 40-XVP scanning electron microscope (SEM) on gold-coated samples working at 20 kV.

Secondly, 13 of the samples were characterized by whole rock chemical analyses (major, minor, and trace elements). They were conducted by Bureau Veritas Laboratories following their standardized procedures (LF200) by inductively coupled plasma emission and mass spectrometry (ICP-ES and ICP-MS). In order to evaluate element mobility (Christidis, 1998), the analytical errors informed by Bureau Veritas Laboratories STD SO-19 standard following the LF200 procedure are presented in Table 1.

Finally, textural and chemical studies were performed on carbon-coated polished thin sections by SEM-EDS (energy-dispersive X-ray spectroscopy) and electron probe microanalysis (EPMA) on selected samples, to characterize the main alteration phases. Backscattered electron (BSE) images and compositional maps were obtained using a Carl Zeiss Σigma high resolution FE (field emission) SEM-EDS microscope working at 15 kV.

Microanalyses were performed using a JEOL JXA 8230 microscope equipped with three wavelength dispersive spectrometers (WDS) and one integrated EDS spectrometer. Conditions of measurements were different depending on the phase analyzed. Zeolites, smectites, and glass were measured at 15 kV and 2 nA, with a defocused beam (spot size of 5-10 µm). Feldspars were measured at 15 kV and 10 nA, with a spot size of 1-2 µm. A counting time of 20 s at the peak and 10 s at each background position was used. Correction for matrix effects was made using the ϕ/(ρz) (‘‘phi-rho-z’’) algorithm (H_2O accounted for

hydrous phases). The standards used were albite (Na, Si, and Al), orthoclase (K), wollastonite (Ca), MgO (Mg), barite (Ba), celestine (Se), hematite (Fe), ilmenite (Ti), and pyrolusite (Mn). Carbon-coated polished thin sections (abrasive size up to 1 µm) were utilized.

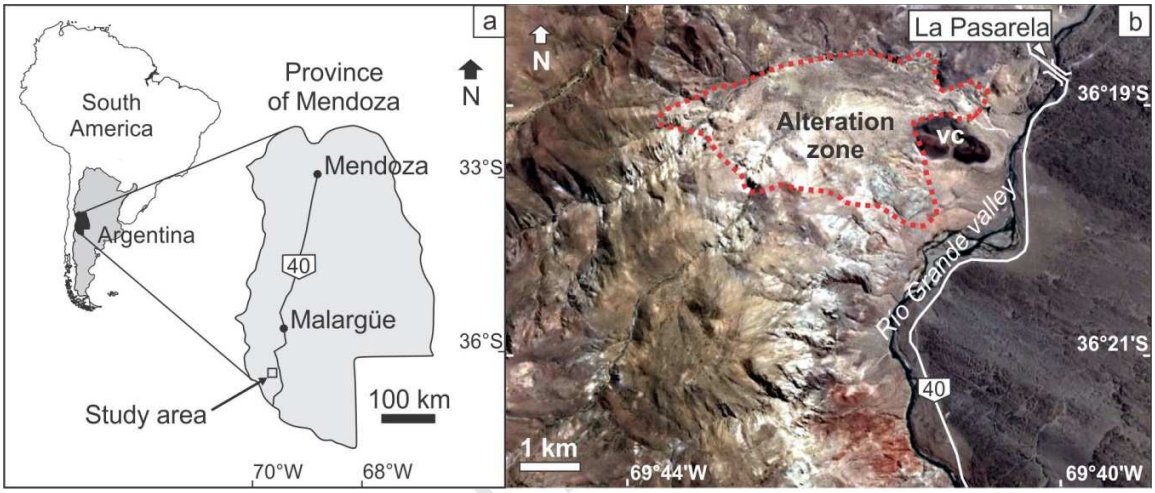

Fig. 1. a) Location of the study area in the province of Mendoza (Argentina). b) The study area is divided into two domains by the Río Grande valley, to the east outcrop the basalts of the western Quaternary Payún Matrú volcanic field (May *et al*., 2018), and to the west Cenozoic volcaniclastic and sedimentary rocks and underlying Cretaceous sediments of the Neuquén Group (Narciso *et al*., 2004). vc: Quaternary monogenetic volcanic cone (Llambías *et al*., 2010).

Standard STD SO-19 (n = 4)

wt%	Mean	*S*	*%S*	*ppm*	Mean	*S*	*%S*	*ppm*	Mean	*S*	*%S*
SiO_2	60.57	0.17	0.28	Co	22.38	1.04	4.66	La	67.21	3.97	5.90
TiO_2	0.69	0.01	0.83	Ga	15.83	0.97	6.11	Ce	148.15	9.89	6.68
Al_2O_3	14.04	0.17	1.22	Rb	18.41	0.71	3.85	Pr	18.52	0.69	3.75

$Fe_2O_3^{(T)}$	7.39	0.12	1.61	Sr	301.86	16.60	5.50	Nd	71.05	2.12	2.98
MnO	0.13	0.00	0.00	Y	34.37	1.52	4.41	Sm	12.42	0.47	3.80
MgO	2.89	0.03	0.87	Zr	108.09	3.24	3.00	Eu	3.46	0.04	1.07
CaO	5.92	0.02	0.40	Nb	67.85	2.99	4.41	Gd	9.93	0.28	2.83
Na_2O	3.99	0.04	1.03	Cs	4.17	0.13	3.01	Tb	1.32	0.04	2.79
K_2O	1.27	0.02	1.44	Ba	464.95	19.31	4.15	Dy	7.08	0.29	4.08
P_2O_5	0.31	0.01	2.63	Hf	3.07	0.10	3.11	Ho	1.31	0.02	1.44
				Ta	4.40	0.14	3.22	Er	3.58	0.09	2.50
				W	9.77	0.81	8.31	Tm	0.51	0.01	1.87
				Th	12.52	0.47	3.77	Yb	3.23	0.06	1.93
				U	18.66	1.45	7.78	Lu	0.50	0.02	4.15

Table 1. Analytical errors for major, minor, and trace elements informed by Bureau Veritas Laboratories STD SO-19 standard, following LF200 procedure. *n* = number of analyses, *S* = standard deviation, *%S* = percentage standard deviation

3. RESULTS

3.1 Geological setting and geochemical characterization

The host rocks of the mineralization are composed of breccias (autobreccias) of light green color (Fig. 2 a-b), where vitreous particles are abundant, especially perlitic, spherulitic and fibrous glass, and vitreous lavas.

Altered banks are several meters thick (up to 3-4 m) and are interlayered with vitreous levels (up to 5-10 m). According to Bengochea *et al*. (1997) the zeolite-bearing rocks cover an area of ~10 km^2 and in the best exposed sectors they can be more than 40 m thick. The brecciation processes produced irregular banks with variable permeability, evidenced by

the irregularity of the mineralization. They discordantly overlie the Upper Cretaceous sediments of the Neuquén Group (Fig. 2 c) and are covered by Tertiary basalts (Molle Eruptive Cycle, MEC) and Quaternary sediments (Fig. 2 d). The breccias are associated with perlitic and spherulitic glass (Fig. 2 e-f), and high-viscosity lavas, which generally form subvertical dikes (Fig. 2 g), and subhorizontal lava flows (Fig. 2 h). In some areas, hydrocarbons penetrate glass fractures. Both glass and lavas related to the alteration are rhyolitic in composition (Fig. 3 a).

According to Narciso *et al*. (2004), in the area outcrops Huincán Formation, consisting of hornblendiferous andesites and pyroclastites of Upper Miocene - Pliocene age. Nullo *et al*. (2002) and Combina and Nullo (2011) located in the area the retroarc MEC (Molle, Puntilla del Huincán and Palaoco basalts) of Lower to Middle Miocene age. They considered that Huincán and La Brea andesites correspond to two magmatic pulses belonging to a later cycle of volcanic arc phase (Huincán Eruptive Cycle, HEC) outcropping north of the studied sector. Some dikes and sills of andesites have been found in the study area, possibly associated with this cycle.

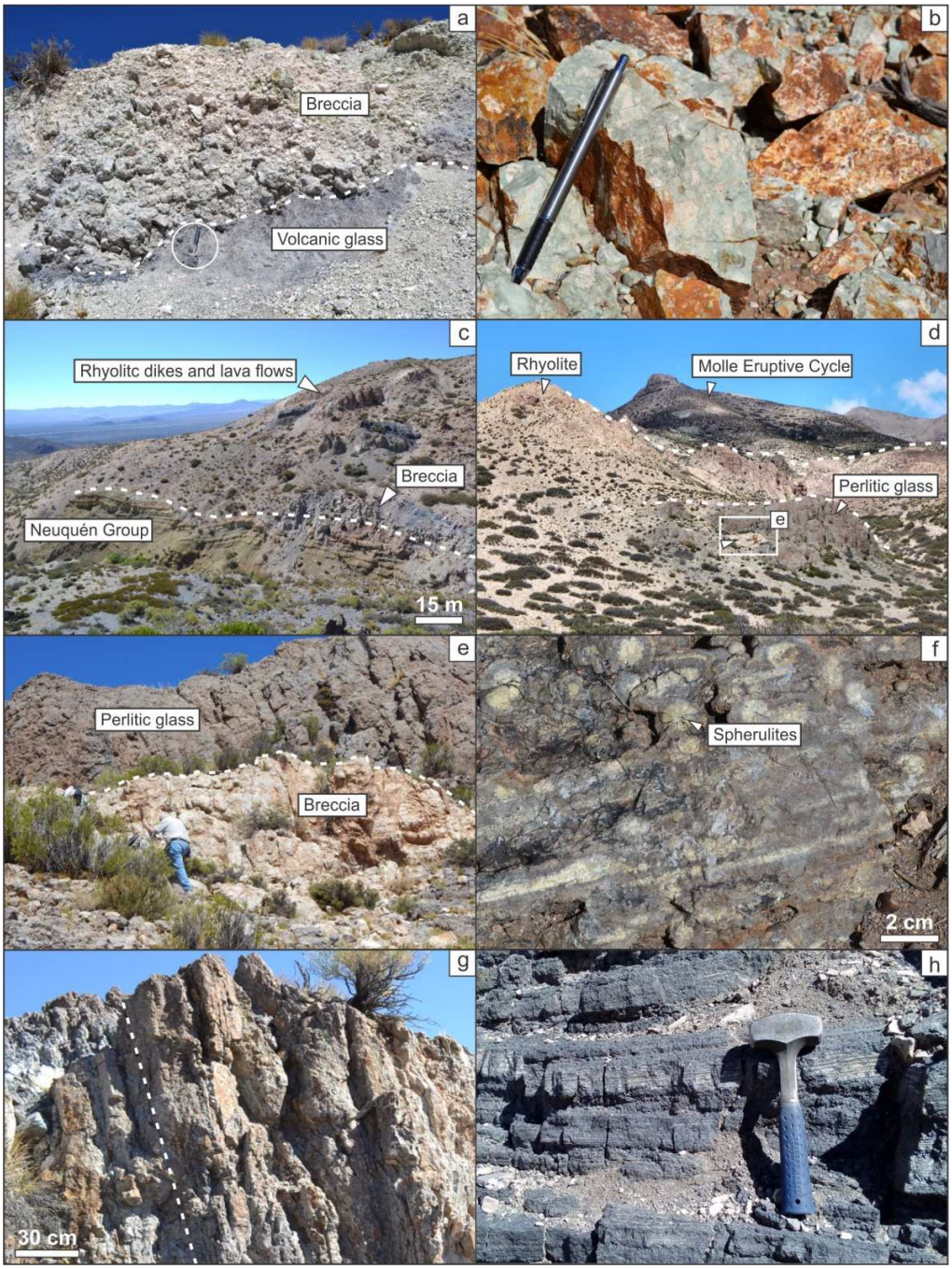

Fig. 2. a) Zeolite-rich breccia over volcanic glass. b) Macroscopic texture of the mineralized rock. c) Breccia associated with dikes and lava flows of rhyolitic composition, and underlying sediments of Neuquén Group. d) Rocks from MEC covering all the

sequence. e) Breccia associated with perlitic glass. f) Detail of spherulitic glass. g) Zeolite-rich breccia associated with subvertical rhyolite dikes. h) Subhorizontal lava flows.

Sruoga *et al.* (2008) studied some volcanites from Cordón del Burrero Volcanic Complex (CBVC) in the province of Mendoza, ~150 km northwest of the study area. They mainly recognized basalts and subordinate andesites and rhyolites of Lower to Middle Miocene age geochemically assigned to high-K calc-alkaline series. According to Combina and Nullo (2011) these rocks could be part of the MEC.

In the absence of geochronological information, geochemical data from the rocks analyzed in this study (Table 2) were compared to those from Molle and Puntilla del Huincán basalts and tuff (MEC) and Huincán andesites (HEC) because they constitute the most proximal (areal and chronological) volcanites (Nullo *et al*., 2002). Also, rhyolites of the CBVC (Suroga *et al*., 2008) were compared to the studied rocks in order to establish their geochemical affinity. Although altered rocks should not be plotted in the geochemical diagrams (Fig. 3), they were included in order to compare them with the non-altered samples.

The geochemical composition of the rocks under study (Fig. 3 a-c) corresponds to subalkaline, calc-alkaline magmas rich in K (non-altered samples plot in the high-K calc-alkaline field), emplaced in a tectonic environment of active volcanic arc (Fig. 3 d). Non-altered samples show geochemical characteristics comparable to rhyolites from CBVC. The chondrite-normalized rare earth element (REE) diagram shows enrichment in low rare earth elements (LREE) and negative europium anomaly (Fig. 3 e). This anomaly is also

evidenced in rhyolites from CBVC, and one sample has the same REE pattern as the samples in this study.

The basalts and andesites of MEC show important differences in the REE content and do not present a negative europium anomaly (Fig. 3 e). This is manifested even in Punta del Huincán dacitic tuff facies, which would indicate that both magmas would not have the same origin. Huincán andesites (HEC) have a REE pattern similar to the rocks of the MEC, except for one sample that is richer in REE and shows negative europium anomaly.

Samples	Fresh obsidian						Partially altered obsidian			Altered breccia			
	2	3	4	5	6	11	1	13	9	7	8	10	12
wt%													
SiO_2	72.93	72.89	72.56	72.56	73.05	73.65	73.94	70.86	70.27	70.18	68.28	68.05	69.27
TiO_2	0.11	0.11	0.11	0.11	0.11	0.10	0.10	0.10	0.10	0.10	0.09	0.10	0.09
Al_2O_3	12.42	12.58	12.53	12.33	12.63	12.55	10.85	12.14	12.64	11.60	11.33	11.36	10.93
$Fe_2O_3^{(T)}$	0.78	0.75	0.78	0.75	0.81	0.77	0.51	0.71	0.79	0.70	0.69	0.83	0.74
MnO	0.07	0.13	0.07	0.06	0.07	0.07	0.01	0.05	0.06	0.03	0.01	0.02	0.01
MgO	0.13	0.14	0.15	0.14	0.16	0.16	0.10	0.13	0.34	0.24	0.39	0.31	0.27
CaO	0.86	0.95	0.94	1.21	0.84	0.83	1.69	1.38	1.74	2.11	2.27	2.66	2.61
Na_2O	3.37	3.28	3.39	3.34	3.10	3.06	1.97	3.59	2.08	1.73	1.47	1.16	1.43
K_2O	4.01	3.98	3.78	3.54	4.60	4.05	3.81	2.26	3.13	2.75	2.86	2.44	2.18
P_2O_5	0.01	0.01	0.02	0.02	0.01	<0.01	0.02	0.02	0.01	0.01	0.02	0.01	0.01
LOI	5.20	5.10	5.50	5.90	4.50	4.60	6.90	8.40	8.70	10.40	12.30	12.90	12.30
Total	99.89	99.92	99.83	99.96	99.88	99.84	99.90	99.64	99.86	99.85	99.71	99.84	99.84
ppm													
Co	0.5	0.6	0.3	0.4	0.3	0.4	0.4	0.5	0.4	0.4	<0.2	0.4	0.5
Ga	12	13.3	12.4	12.4	12.8	12.2	10.2	12.8	13.3	11.6	10.5	12	10.4
Rb	156.6	152.8	129.7	124.4	131.9	136.7	84.2	124	124.1	133.2	105.7	116.2	128

Sr	140.1	143.5	131.2	161.5	130.2	142.8	189	642.5	209.2	299.9	639.9	467	380.8
Y	13	12.5	12.3	12.9	13.1	12.6	12.4	11.8	11	10.5	10.2	9.9	10
Zr	75.1	76.3	76.2	77	83.2	75.8	78.2	70.8	73.3	68.4	63	60.9	60.2
Nb	17.9	18.3	17.6	17.5	18.2	17.6	14.6	16.2	15.7	18.3	16.2	22	17.1
Cs	6	8.7	5.3	5.7	4.1	3.7	10.6	56.4	4.9	7.3	5.8	6.7	8.3
Ba	717	701	677	688	702	730	488	654	488	568	1221	798	569
Hf	2.6	2.7	2.6	2.7	2.7	2.7	2.6	2.5	2.5	2.2	2.4	2.4	2.2
Ta	1.7	1.6	1.5	1.6	1.7	1.7	1.6	1.4	1.6	1.4	1.3	1.1	1.6
W	2.9	1.8	1.3	1.3	1.2	<0.5	3.5	0.7	<0.5	0.5	1.5	1.7	0.8
Th	12.1	12	11.7	11.7	11.9	11.9	10.3	11.5	11.6	10.6	10	10.2	9.8
U	3.1	3.4	3.5	3.4	3.7	3.6	2.3	3.4	3	2.2	2.2	0.5	1
La	25.7	26.3	24.6	25.1	25.3	26.9	21.6	25.1	25.1	25.3	22.4	24.5	23.2
Ce	44	43.8	43	43.7	42.9	47.1	37.3	44.9	44.7	43.9	37.3	41	42.6
Pr	4.68	4.77	4.6	4.56	4.69	4.68	4.07	4.56	4.45	4.41	3.81	4.13	4.22
Nd	14.7	15.4	14.7	15.2	15.1	14.7	13.6	14.9	14.6	14.2	12	13.1	12.9
Sm	2.45	2.54	2.38	2.39	2.47	2.37	1.97	2.33	2.29	2.1	1.87	2.11	2.35
Eu	0.43	0.46	0.43	0.41	0.41	0.41	0.39	0.41	0.38	0.37	0.34	0.34	0.4
Gd	1.99	2.18	2	2.06	2.09	1.96	1.74	2.13	1.89	1.83	1.76	1.71	1.72
Tb	0.32	0.33	0.31	0.32	0.33	0.31	0.28	0.33	0.29	0.28	0.25	0.28	0.28
Dy	1.99	1.94	1.91	1.86	2.02	1.98	1.81	1.74	1.67	1.77	1.51	1.61	1.68
Ho	0.39	0.43	0.4	0.41	0.41	0.39	0.41	0.38	0.35	0.42	0.33	0.3	0.31
Er	1.25	1.29	1.24	1.32	1.36	1.32	1.25	1.12	1.03	1.06	1.03	0.96	1.1
Tm	0.2	0.2	0.2	0.21	0.21	0.19	0.21	0.2	0.17	0.17	0.15	0.15	0.17
Yb	1.45	1.47	1.4	1.39	1.48	1.4	1.47	1.39	1.13	1.12	1.12	1	1.07
Lu	0.23	0.23	0.22	0.24	0.24	0.24	0.24	0.24	0.17	0.2	0.19	0.15	0.17

168 Table 2. Whole-rock data of the studied samples. LOI: loss on ignition.

169

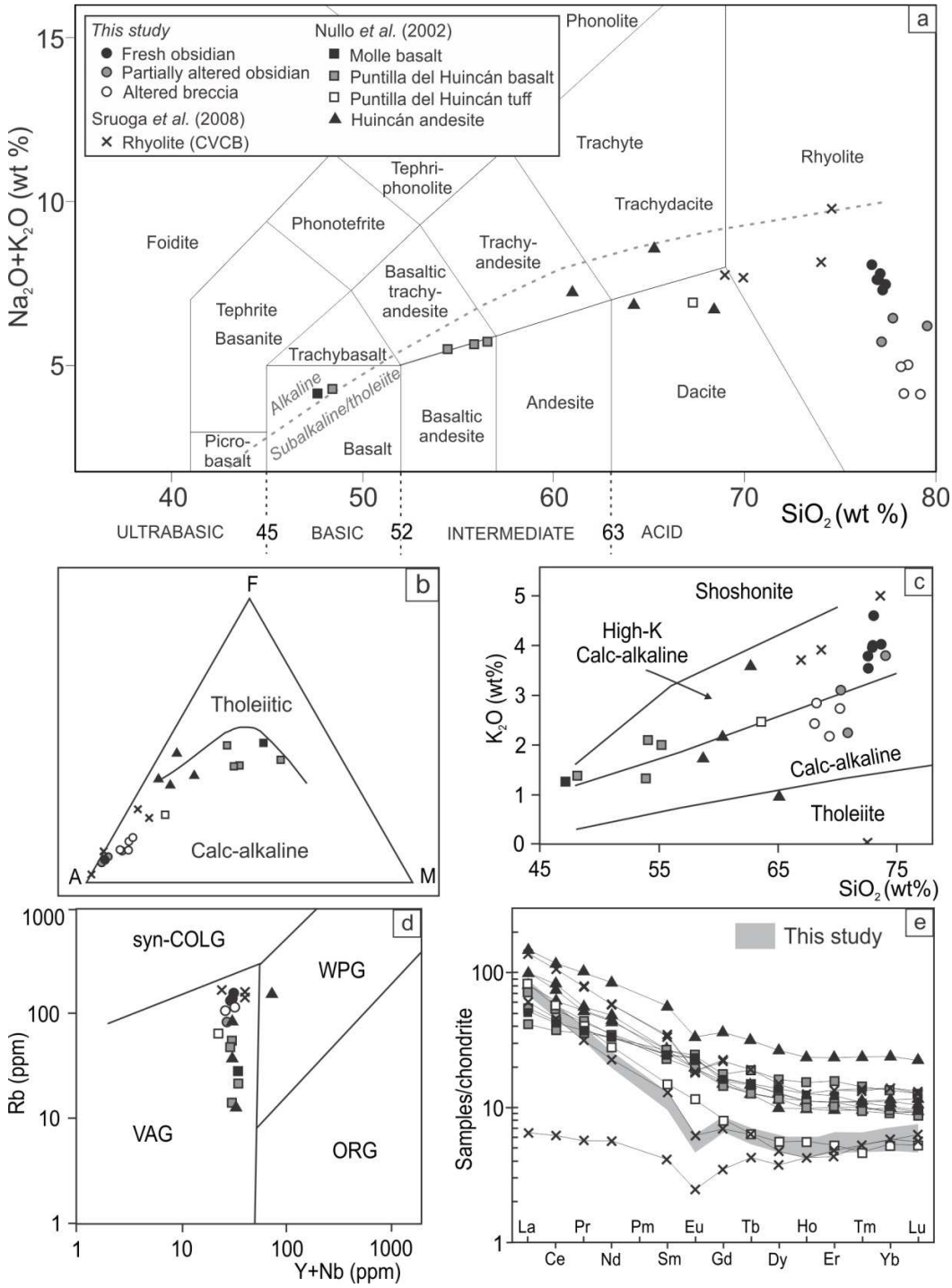

170

171 Fig. 3. a) Total alkali silica (TAS) diagram for the chemical classification of volcanic rocks

172 (Le Bas *et al.*, 1986). The dashed curve divides alkaline from subalkaline/tholeiite series

(Irvine and Baragar, 1971). b) AFM diagram (A: Na_2O+K_2O, F: FeO_{total}, M: MgO) to discriminate between calc-alkaline and tholeiite series (Irvine and Baragar, 1971). c) K_2O vs. SiO_2 diagram for subdivision of subalkaline rocks (Peccerillo and Taylor, 1976). d) Rb-(Y+Nb) discrimination diagram for granites (Pearce *et al.*, 1984) showing the fields of syn-collisional granites (syn-COLG), within-plate granites (WPG), volcanic-arc granites (VAG), and ocean-ridge granites (ORG). e) Chondrite-normalized REE diagram (Boynton, 1984).

3.2 Characterization of the mineralized breccias

The mineralized breccia is composed of angular to subangular vitreous clasts of variable size (~3 cm to < 100 µm), partially welded, defining sectors of variable porosity (Fig. 4 a). Glass fragments are massive or show fibrous, perlitic and spherulitic textures, sometimes associated with evidence of magmatic flow (Fig. 4 b). Spherulites are typical of devitrification processes (tridymite/cristobalite and potassium feldspar intergrowth), while the perlitic texture corresponds to curved cracks that surround cores of fresh glass typically associated with strain induced by hydration (McPhie *et al*., 1993). Pumice fragments are also observed. Scarce euhedral plagioclase crystals and subrounded lithoclasts of andesites and andesitic tuff with vitreous matrix (partially or totally devitrified and altered), and ignimbrites were also identified (Fig. 4 c). Concentric cracks were recognized in the surrounding glass of some spherulites (Fig. 4 d). Perlitic cracks can affect the fresh glass (Fig. 4 b and d) but they were also observed on a partially welded matrix and glass clasts in the breccias (Fig. 4 e). Traces of oil were recognized associated with perlitic cracks (Fig. 4 f).

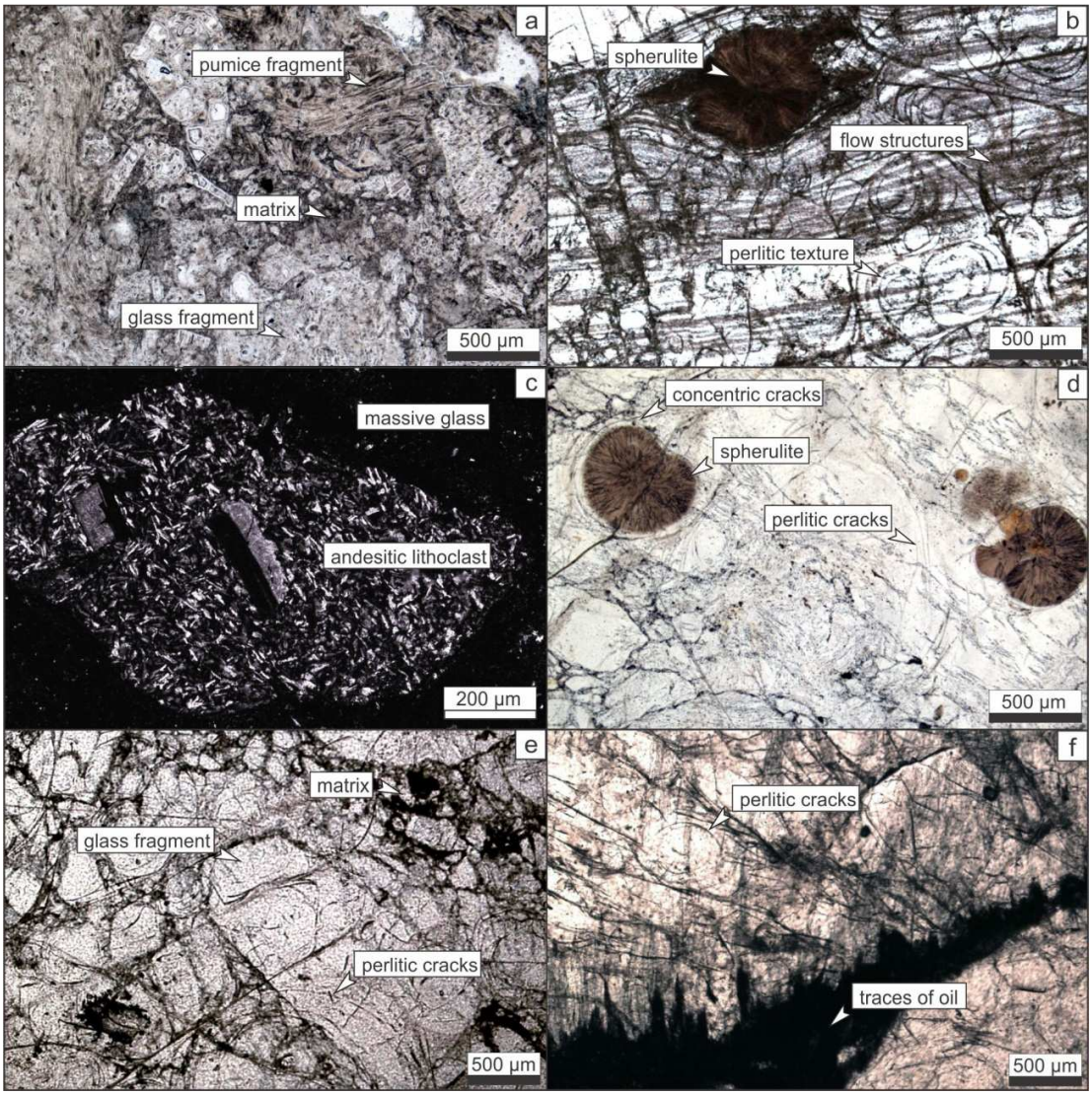

Fig. 4. Photomicrographs. a) Texture of the mineralized breccia with angular to subangular fragments of glass in a very fine-grained matrix (N//). b) Fragment with perlitic-spherulitic texture. Structures of magmatic flow are recognized (N//). c) Andesitic lithoclast in massive glass (NX). d) Spherulites with concentric cracks (N//). e) Breccia with perlitic cracks affecting glass fragments and partially welded matrix (N//). f) Traces of oil associated with perlitic cracks (N//).

Fibrous mordenite and fine-grained smectites were observed as replacement in perlitic cracks (Fig. 5 a-b). More porous samples show intense alteration, with development of fine-grained zeolites and clay minerals in the matrix, and well-developed crystals filling cracks and vesicles (Fig. 5 c-e). In general, very fine-grained smectites of high interference color cover the cavities, and later, two generations of well-formed zeolites, characterized by low-interference colors, grow as open-space fillings. Fibrous mordenite represents the first generation, and pseudohexagonal prismatic and tabular clinoptilolite the second one. Later veins of colloform silica and small euhedral crystals of secondary feldspar (interpreted as adularia) were also recognized crosscutting the altered rock (Fig. 5 f and 6 f). Petrography and XRD analyses (Fig. 5 g) confirmed that the most altered samples are composed mainly of mordenite with a small amount of relicts of volcanic glass, potassium feldspar (adularia and probably orthoclase from spherulites), opal-CT ± colloform silica, plagioclase, smectite, and clinoptilolite. This last phase was only recognized in the most altered samples.

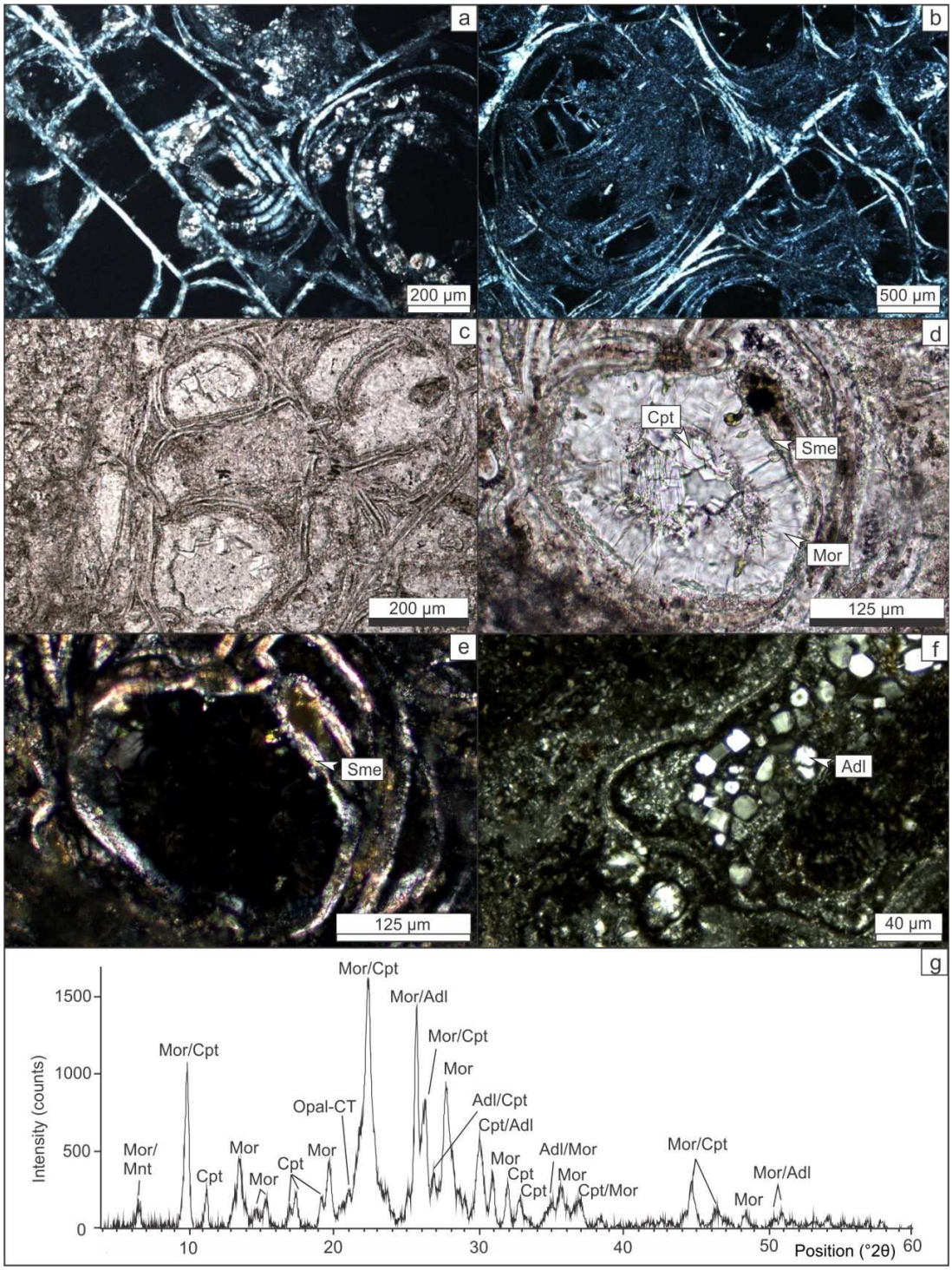

Fig. 5. Photomicrographs (a-f) and XRD pattern (g). a) Perlitic glass with fibrous mordenite and fine-grained smectites in perlitic cracks (NX). b) The same alteration process in a

partially altered perlitic glass (NX). c) More porous glass fragment with alteration minerals in cracks and cavities (N//). d) Detail of a cavity filled with smectite, mordenite, and clinoptilolite (N//). e) Same sector at NX. f) Colloform silica associated with small euhedral crystals of adularia in a vein (NX). g) XRD pattern of the most altered breccia.

The morphology of fibrous mordenite and prismatic clinoptilolite in cavities, and laminar smectite (flakes) formed from volcanic glass is clearly differentiated by SEM (Fig. 6 a-c). Mordenite constitutes the main alteration phase of the breccia. It is found in the matrix of the rock and as replacement of glass particles, generating a patchy texture (patches of relict volcanic glass in a fine-grained mordenite mass) recognizable in BSE images (Fig. 6 d and f, Fig. 7). Highly vesicular pumice fragments show well-developed crystals in the cavities. Some vesicles are filled with fibrous mordenite followed by prismatic clinoptilolite, whereas smectite is restricted to the cavity boundaries (as mentioned in Fig. 5 d-e). In other parts, vesicles are filled with fine-grained smectites and/or later massive or prismatic clinoptilolite, and mordenite replaces vesicle walls (Fig. 6 d and e). When present, clinoptilolite clearly crystallized after mordenite. Smectite is scarce but ubiquitous, and generally represents the earliest alteration phase. Although adularia veins are the last alteration phase (crosscutting the mineralized breccia texture), other K-feldspars were recognized growing at the plagioclase boundaries (Fig. 7). However, correlation with adularia veins could not be performed.

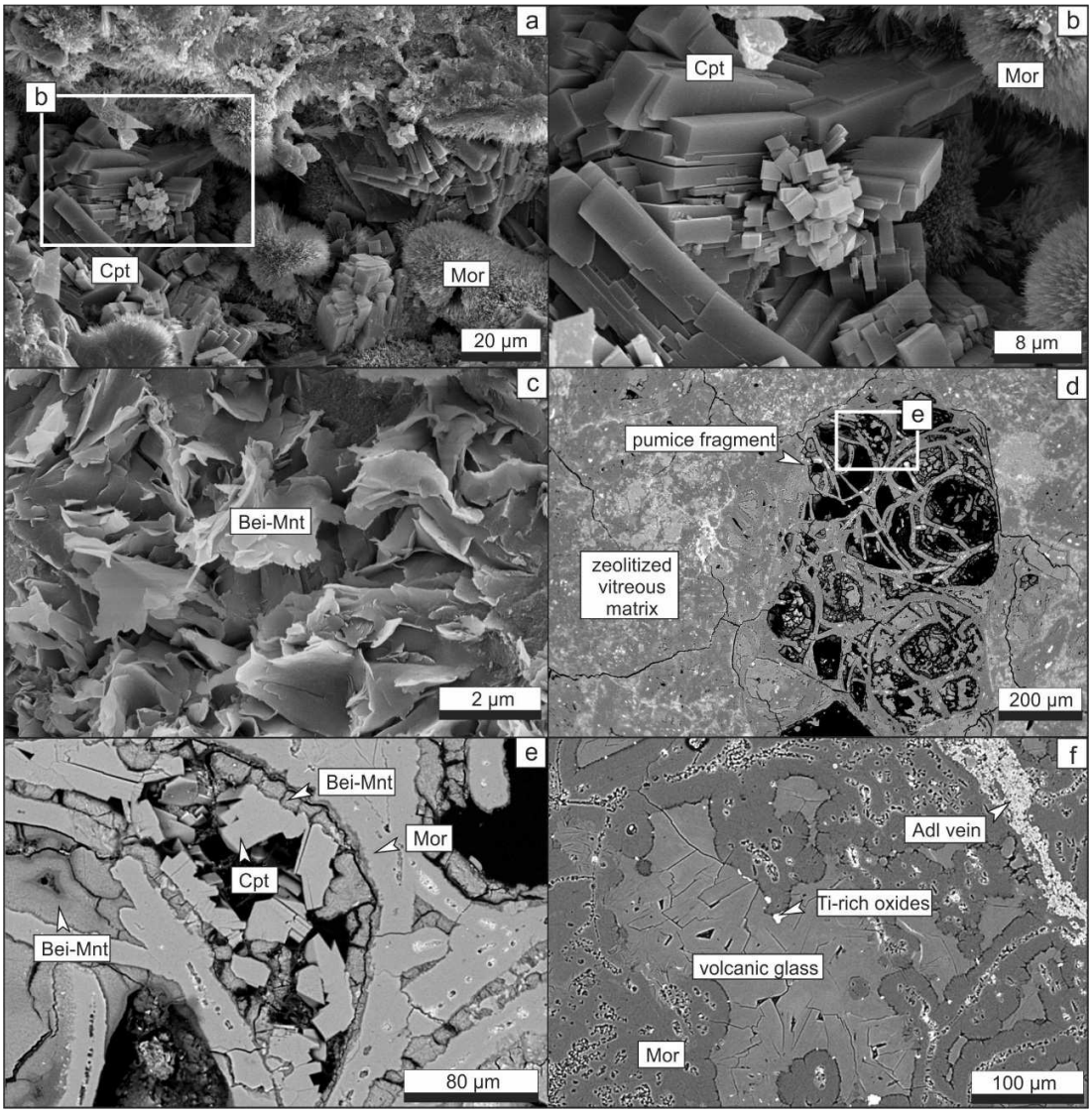

Fig. 6. a) Cavity with prismatic clinoptilolite and fibrous mordenite (SE-SEM). b) Detail of sector "b" (SE-SEM). c) Flakes of smectite formed from volcanic glass (SE-SEM). d) Altered pumice fragment in a zeolitized vitreous matrix (BSE-EPMA). e) Detail of sector "e" indicated in 6-9 d. Vesicles are filled with fine-grained smectite and prismatic clinoptilolite. Vesicle walls were replaced by mordenite (BSE-EPMA). f) Volcanic glass

248 partially replaced by mordenite (patchy texture). Veins of adularia crosscutting the rock are
249 also common (BSE-EPMA).

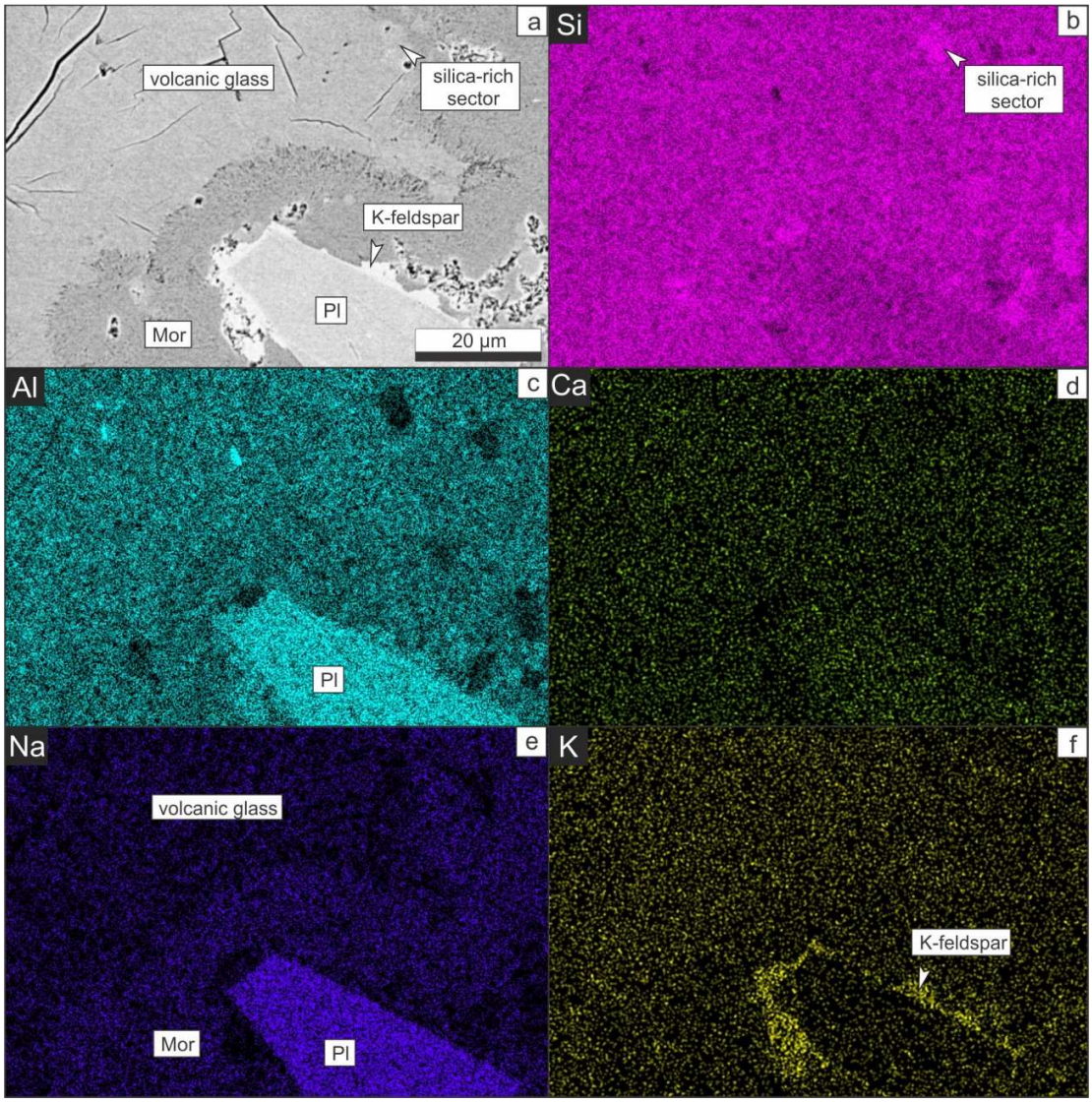

250

251 Fig. 7. a) Volcanic glass partially replaced by mordenite. In the image a plagioclase crystal
252 with recrystallization of K-feldspar at the edges can also be seen (BSE-SEM). b-f)
253 Compositional maps of Si (b), Al (c), Ca (d), Na (e), and K (f) in the same sector (SEM-
254 EDS).

255

EPMA confirmed the rhyolitic composition of the glass (Table 3). Adularia in veins and K-feldspars growing over plagioclase have similar composition (Ab = 2.19%, An = 1.93%, Or = 95.88%; Table 3). Smectites are dioctahedral (Table 3) and belong to the montmorillonite-beidellite series (Fig. 8 a). Although local chemical variations were detected (local enrichment in Al or Si), no compositional zonation or clear pattern was observed to explain such variations (Fig. 6 e). Plagioclase corresponds to oligoclase (Ab = 73.30%, An = 21.53%, Or = 5.17%; Table 3). According to the Na^{+}-K^{+}-M^{2+} diagram, zeolites are classified as Ca-K-rich clinoptilolites and Ca-Na-rich mordenites (or Ca-Na-K-rich), similar to the analyses reported by Ghiara *et al*. (1999) (Table 4 and Fig. 8 b). Only analyses with *E%* (Gottardi and Galli, 1985; Campbell *et al.*, 2016) between +10 and -10 are presented in Table 4 and Fig. 8 a and b. *R* values are in agreement with the ranges proposed by Passaglia and Sheppard (2001) for clinoptilolite (0.73-0.85) and mordenite (0.80-0.86).

In Fig. 8 c volcanic glass is compared to the principal alteration phases as a function of the main oxides. It can be seen that clinoptilolite is similar in composition to volcanic glass but mordenite has higher SiO_2/Al_2O_3 and $Na_2O+K_2O/Na_2O+K_2O+CaO$ ratios. This difference is evidenced in the compositional maps, mainly due to the higher Na content in mordenite compared to volcanic glass (Fig. 7 e). Finally, chemical differences between smectites and volcanic glass are significant, due to the low SiO_2 and high Al_2O_2 content, and the low $Na_2O+K_2O/Na_2O+K_2O+CaO$ ratio of the former, but mainly because of the high content of Fe_2O_3 and MgO (Table 2).

279

280

Volcanic glass/Mineral	Volcanic glass		Plagioclase		K-feldspar			Beidellite-montmorillonite	
No. of analyses	10		4		4			9	
	Mean	*s*	Mean	*s*	Mean	*s*		Mean	*s*
SiO_2	71.13	1.21	63.59	1.35	67.90	0.76		58.66	2.86
TiO_2	0.00	0.00	0.12	0.24	0.13	0.26		0.27	0.23
Al_2O_3	12.88	0.18	22.95	1.22	16.62	0.37		25.90	2.76
Fe_2O_3(*)	0.03	0.05	0.26	0.09	1.13	0.75		1.84	0.23
MnO	0.03	0.09	0.04	0.08	0.02	0.04		0.43	0.41
MgO	0.68	0.14	0.02	0.03	0.13	0.11		1.95	0.73
CaO	3.28	0.24	4.24	0.68	0.31	0.15		2.14	0.40
Na_2O	0.51	0.16	7.98	0.62	0.19	0.13		0.07	0.04
K_2O	2.25	0.28	0.85	0.26	12.83	0.85		1.01	0.18
Total	90.79	1.33	100.05	0.50	99.26	0.59		92.26	4.03
apfu									
Si			2.809	0.047	3.094	0.029		3.755	0.100
Ti			0.004	0.008	0.004	0.009		0.013	0.011
Al			1.195	0.068	0.893	0.016		1.953	0.185
Fe^{3+}			0.009	0.003	0.039	0.026		0.089	0.014
Mn			0.001	0.003	0.001	0.002		0.023	0.022
Mg			0.001	0.002	0.009	0.008		0.186	0.068
Ca			0.201	0.033	0.015	0.008		0.147	0.024
Na			0.683	0.050	0.017	0.012		0.009	0.005
K			0.048	0.015	0.746	0.049		0.083	0.014
Σ(cation)			4.951	0.001	4.817	0.015		6.257	0.014
end member (%)							ΣOct.	2.019	
Ab			73.30		2.19		ΣInt.	0.238	

An	21.53	1.93	Charge	0.384
Or	5.17	95.88		

Table 3. Chemical analyses of volcanic glass, feldspars, and smectites by EPMA. Component contents expressed as weight percent (wt%) of oxides. Atoms per formula unit (apfu) were calculated on the basis of 8 oxygen atoms for feldspars and 11 for smectites. (*) Fe_2O_3: iron concentration recalculated as total Fe_2O_3. b.d.l.: values below the detection limit (twice the equipment detection limit).

Mineral	Clinoptilolite							Mordenite			
SiO_2	68.88	69.49	69.52	68.53	68.86	68.99	70.40	72.23	73.60	73.81	74.73
Al_2O_3	13.44	12.96	13.70	13.66	13.62	13.19	13.11	11.11	11.59	11.42	11.44
Fe_2O_3	b.d.l.	0.00	b.d.l.	0.00	0.00	0.00	0.08	0.00	0.00	b.d.l.	b.d.l.
MnO	b.d.l.	b.d.l.	0.00	0.00	0.20	0.00	0.00	b.d.l.	0.00	0.12	0.10
MgO	0.61	0.82	0.63	0.75	0.66	0.59	0.77	b.d.l.	b.d.l.	b.d.l.	b.d.l.
CaO	4.13	4.11	4.07	3.65	3.95	3.97	2.74	3.24	3.35	3.11	3.00
BaO	0.20	0.66	0.61	0.30	0.77	0.58	0.18	0.11	0.27	0.00	b.d.l.
SrO	0.56	0.28	0.60	0.37	0.31	b.d.l.	0.11	0.00	b.d.l.	0.00	b.d.l.
Na_2O	0.54	0.52	0.32	0.39	0.56	0.61	1.06	1.42	1.69	2.21	1.94
K_2O	3.03	2.24	2.18	2.80	2.74	2.52	3.36	1.87	2.12	1.98	1.95
Total	91.38	91.07	91.62	90.46	91.67	90.45	91.81	89.98	92.62	92.65	93.16
apfu											
Si	29.223	29.455	29.300	29.242	29.172	29.417	29.564	40.745	40.520	40.572	40.738
Al	6.720	6.474	6.805	6.869	6.800	6.628	6.488	7.386	7.520	7.398	7.349
Fe^{3+}	0.000	0.000	0.000	0.000	0.000	0.000	0.025	0.000	0.000	0.000	0.000
Σ T	35.943	35.929	36.104	36.111	35.972	36.045	36.077	48.130	48.039	47.970	48.087

Mn	0.000	0.000	0.000	0.000	0.071	0.000	0.000	0.000	0.000	0.055	0.046
Mg	0.384	0.516	0.394	0.477	0.418	0.377	0.483	0.000	0.000	0.000	0.000
Ca	1.877	1.866	1.838	1.669	1.793	1.814	1.233	1.958	1.976	1.831	1.752
Ba	0.034	0.109	0.101	0.050	0.128	0.097	0.029	0.025	0.059	0.000	0.000
Sr	0.137	0.068	0.146	0.093	0.077	0.000	0.026	0.000	0.000	0.000	0.000
Na	0.442	0.426	0.258	0.325	0.458	0.501	0.864	1.553	1.804	2.355	2.050
K	1.640	1.211	1.172	1.524	1.481	1.371	1.800	1.346	1.489	1.388	1.356
Σ EC	4.514	4.197	3.909	4.137	4.425	4.159	4.434	4.881	5.327	5.630	5.204
R	0.813	0.820	0.812	0.810	0.811	0.816	0.820	0.847	0.843	0.846	0.847
E%	-3.26	-4.19	6.53	6.91	-1.62	2.80	4.97	7.60	2.14	-1.58	4.97

Table 4. Chemical analyses of zeolites by EPMA. Component contents expressed as weight percent (wt%) of oxides. Atoms per formula unit (apfu) were calculated on the basis of 72 and 96 oxygen atoms for clinoptilolite and mordenite respectively. (*) Fe_2O_3: iron concentration recalculated as total Fe_2O_3. b.d.l.: values below the detection limit (twice the equipment detection limit). R = Si/(Si+Al). $E\%$ = 100 × [(Al + Fe^{3+}) – (ΣM^{+}) – 2(ΣM^{2+})]/[(ΣM^{+}) + 2(ΣM^{2+})], charge balance according to Gottardi and Galli (1985) and Campbell *et al.* (2016).

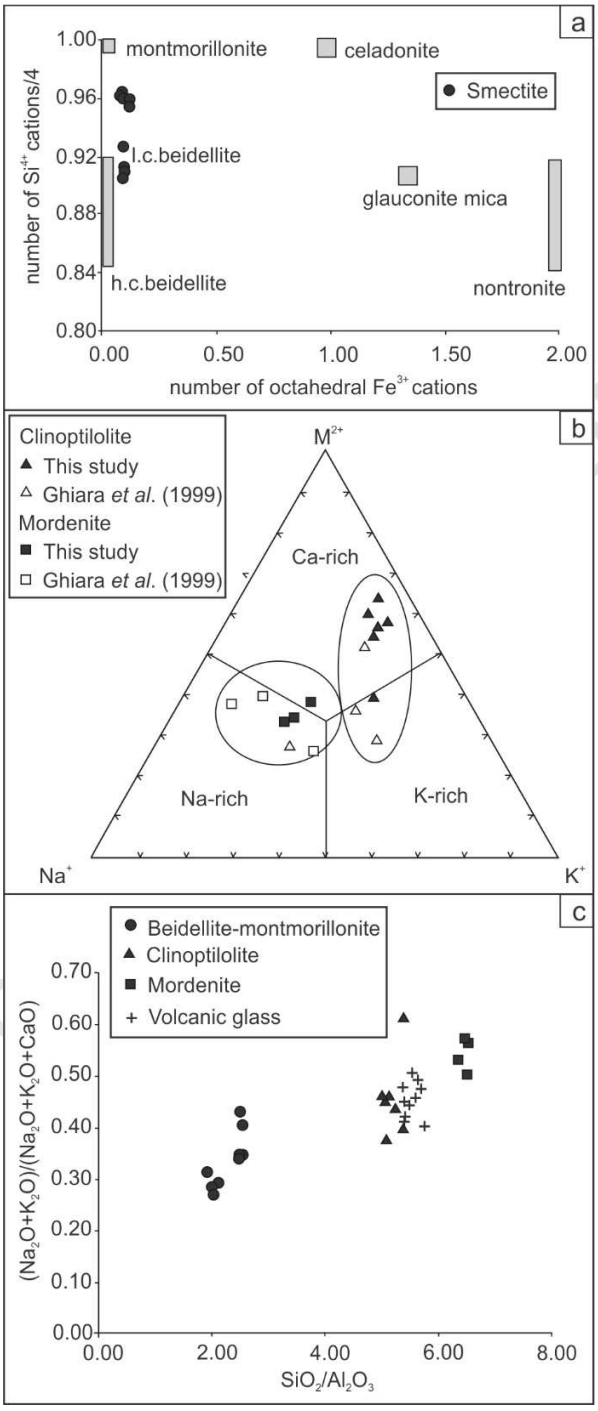

296

297 Fig. 8. a) Classification of smectites in the diagram $Si^{4+}/4$ vs. octahedral Fe^{3+} (apfu).
298 Compositional fields for dioctahedral smectites (gray) adapted from Meunier (2005). b)
299 M^{2+}-Na^{+}-K^{+} ternary plot to evaluate zeolite chemistry (apfu). M^{2+}: Ca + Mg + Mn + Ba +

Sr. Values from Ghiara *et al*. (1999) were plotted as empty signs for comparison. c) Chemical comparison (wt% of oxides) between volcanic glass and alteration products (beidellite-montmorillonite, clinoptilolite, and mordenite).

3.3 Behavior of major, minor, and trace elements during the alteration

Chemical mobility of major, minor, and trace elements during the alteration process was analyzed by the isocon method (Grant, 1986, 2005). In this paper, the normalization solution proposed by Guo *et al*. (2009) was chosen, in order to illustrate the mobility of multiple progressively altered samples (fresh obsidian, partially altered breccia, altered breccia). The Al_2O_3 was assumed to be the most immobile major element in the system. Considering that there is not a unique alteration profile in the outcrop, mean values of the fresh obsidians (6 samples), partially altered breccias (3 samples) and altered breccias (4 samples) were used in the application of the method. Mean values for each group (fresh, partially altered, and altered), normalizing factors, and normalized data are presented in Table 5. Finally, normalized data for the altered samples were plotted against data of fresh samples (Fig. 9). In order to improve the visualization of the isocon diagrams, different scaling factors were used as suggested by Grant (1986, 2005). The scaling factors are listed in Table 5.

319

	Original data (mean values)			Normalized data			
	Fresh obsidian (n = 6)	Partially altered breccia (n = 3)	Altered breccia (n = 4)	Fresh obsidian (n = 6)	Partially altered breccia (n = 3)	Altered breccia (n = 4)	Scaling factors
wt%							
SiO_2	72.94	71.69	68.95	72.94	71.69	72.43	0.25
TiO_2	0.11	0.10	0.10	0.11	0.10	0.10	150
Al_2O_3	12.51	11.88	11.31	12.51	11.88	11.88	2
$Fe_2O_3^{(T)}$	0.77	0.67	0.74	0.77	0.67	0.78	28
MnO	0.08	0.04	0.02	0.08	0.04	0.02	65
MgO	0.15	0.19	0.30	0.15	0.19	0.32	90
CaO	0.94	1.60	2.41	0.94	1.60	2.53	11
Na_2O	3.26	2.55	1.45	3.26	2.55	1.52	2.9
K_2O	3.99	3.07	2.56	3.99	3.07	2.69	1.7
P_2O_5	0.01	0.02	0.01	0.01	0.02	0.01	100
LOI	5.13	8.00	11.98	5.13	8.00	12.58	0.6
ppm							
Co	0.42	0.43	0.43	0.42	0.43	0.46	30
Ga	12.52	12.10	11.13	12.52	12.10	11.69	2.1
Rb	138.68	110.77	120.78	138.68	110.77	126.88	0.015
Sr	141.55	346.90	446.90	141.55	346.90	469.50	0.06
Y	12.73	11.73	10.15	12.73	11.73	10.66	0.86
Zr	77.27	74.10	63.13	77.27	74.10	66.32	0.1
Nb	17.85	15.50	18.40	17.85	15.50	19.33	0.2
Cs	5.58	23.97	7.03	5.58	23.97	7.38	1.1
Ba	702.50	543.33	789.00	702.50	543.33	828.90	0.03
Hf	2.67	2.53	2.30	2.67	2.53	2.42	5.6
Ta	1.63	1.53	1.35	1.63	1.53	1.42	11

W	1.70	2.10	1.13	1.70	2.10	1.18	0.5
Th	11.88	11.13	10.15	11.88	11.13	10.66	2
U	3.45	2.90	1.48	3.45	2.90	1.55	1.5
Normalizing factor		11.88/11.88	11.88/11.31				

Table 5. Data used for the normalized isocon diagrams (following the procedure of Guo *et al*., 2009). Original data (mean values of fresh obsidians, partially altered breccias, and altered breccias) and normalized data are presented (after multiplying by the normalizing factors).Scaling factors used for plotting are shown in the last column.

During alteration, hydration is evidenced by the increment in LOI values, followed by leaching of Mn, K and Na, and enrichment in Ca and Mg. The Fe is scattered, while Si, Ti, Al, and P are essentially immobile. Minor and trace elements show enrichment in Sr during alteration and slight leaching of Hf, Ta, Th, U, while Ba and W are scattered. Although Cs is slightly enriched, the high value observed in the normalized isocon diagram (Fig. 9b) is from one sample (sample 13, 56.4 ppm), which affects the mean value of the partially altered varieties (concentration of Cs is generally ~ 4-11 ppm). The Co, Ga, Rb, Y, Zr, and Nb are considered immobile as their values are within the analytical errors of the measurements (Table 1).

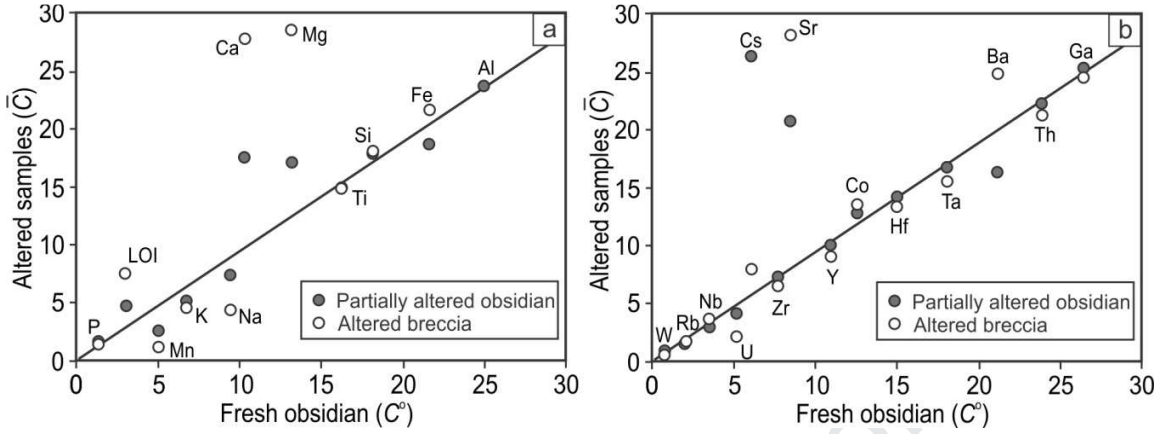

Fig. 9. Normalized isocon diagrams using the normalization solution after Guo *et al*. (2009) for major (a, weight percent) and minor and trace elements (b, ppm). C° represents the compositions of fresh obsidian (mean value of 6 samples). $\bar{C}$ represents the normalized compositions of two altered samples: partially altered breccia (mean value of 3 samples) and altered breccia (mean value of 4 samples). The solid line indicates the unified isocon defined by immobile Al_2O_3. Labels for oxides (a) are abbreviated to the cation elements.

4. DISCUSSION

Multi-analytical studies performed on both fresh and altered samples (petrography, XRD, SEM-EDS analyses, and EPMA) support that the alteration started in the vitreous fragments of the breccias, mainly in the areas where the glass has perlitic texture, recognizing mordenite or smectite (beidellite-montmorillonite series) as the main phases of this stage. In some cavities alternate layers of smectites and mordenite were observed. Therefore, during this stage, the characteristics of the solution could fluctuate favoring one or another phase. Afterwards, clinoptilolite was always formed after mordenite or smectite, mainly in the cavities of pumice fragments (Fig. 6 e). The last stage identified is the

development of adularia-rich veins (and secondary K-feldspar crystallizing at the boundaries of former plagioclase crystals) and colloform silica.

It could be seen that the more permeable the rock (i.e., more brecciated) the more intense the alteration process. Smectite is present in very low amounts, which is in accordance with the low concentration of magnesium in the system. As shown by the chemical analysis, alteration is characterized by the leaching of alkalis and concentration of calcium and little magnesium. Nevertheless, the concentration of alkalis is always higher than that of magnesium. The formation of smectites is promoted by the leaching of alkalis and a high Mg activity (Hay, 1977; Senkayi *et al*., 1984). High ratios of (Na + K)/H activity favor the formation of zeolites instead of smectites (Hess, 1966). Since the activity of Mg is very low, a small amount of smectite would probably form at the early stages, until the Mg activity of the media decreases, rising the $(Na^{+}K^{+}Ca^{2+})/H^{+}$ activity (Ca is already in the solution) and the pH of interstitial solutions, thus favoring the formation of mordenite (Hay & Sheppard, 1977; Christidis, 2001). After glass dissolution and smectite formation, the concentration of the solution must have remained high in silica (high SiO_2:Al_2O_3 ratio), favoring mordenite and other Si-rich phases, such as opal-CT (e.g., Fig. 7). As the Na and K are consumed to form mordenite, the solution becomes rich in Ca and thus Ca-rich clinoptilolite is formed (Fig. 8 b). Some of the potassium that was leached during glass dissolution will later contribute to the formation of adularia that precipitates in veins and open spaces (Fig. 5 f and 6 f) or as rims around former plagioclase crystals (Fig. 7).

During alteration some elements were incorporated (mainly Ca, Mg, Sr) and others partially leached (mainly Na, K, Mn and Hf, Ta, Th, U to a lesser extent), while the other elements remained immobile or showed scattered behaviors. The Na and K were not completely

leached off the system as evidenced in the bulk chemical analyses and microanalyses on mineral phases of the altered samples. The presence of opal-CT and zeolites coexisting with smectites indicates that Si and alkalis (at least in part) were retained in the system. This evidence, in addition to the external influx of Ca, Mg, and Sr, might indicate a semi-open system (Kitsopoulos, 1997). Cs is enriched in two samples, 1 and 13, both partially altered.

The formation temperature of mordenite by synthesis from different precursors ranges between 75ºC and 400ºC (Senderov, 1963; Seki, 1973; Barrer, 1982). The first mordenite synthesis from natural glass was made using powdered silicic obsidian (rhyolitic in composition) that was suspended in the natural hydrothermal fluid of a bore hole at Wairakei, New Zealand. Mordenite was formed at 230, 300 ºC, at 17 days, and slightly acid pH (5.7) (Ellis, 1960).

Mordenite from natural silicic glass has also been reported by Wirsching (1976), Hawkins *et al.* (1978), Kirov *et al.* (1979), and Phillips (1983). These experimental studies indicated that mordenite is favored over clinoptilolite by higher temperatures and higher Na:K ratios of the system. In volcanic rocks, crystallization of the highly siliceous zeolites, clinoptilolite, and mordenite is favored by a highly silicic composition of the original glass (Sheppard *et al.*, 1988) and pH in the range of 7-9 (Mariner and Surdam, 1970; Sheppard *et al.*, 1988).

The rhyolitic composition of glass has been an important factor in zeolite formation. The chemical variations produced during the alteration evidence the external contribution of Ca, Mg, Sr (mainly), and Ba (less marked). The Ca, Ba and Sr have similar geochemical behavior, and the last two replace Ca, mainly in carbonatic rocks. The Mg is common in carbonatic rocks (dolostone type) or associated with Ca in calcite (magnesium calcite).

399 In the study area, carbonatic rocks, with subordinate dolomite, are abundant (Roca and
400 Agrio Formations, etc.). Therefore, a plausible explanation could be that meteoric water
401 would have infiltrated and circulated through those rocks, partially dissolving the
402 carbonatic minerals and getting rich in Ca, Sr and Mg, contributing these elements to the
403 system.

404 The cause of cesium enrichment is not straightforward. Cesium and rubidium follow a
405 general geochemical pathway of potassium. Among different zones of the lithosphere, the
406 highest Cs/K and Cs/Rb ratios (0.16×10^{-3} and 0.04, respectively; McLennan, 2001) occur
407 in the upper continental crust (UCC), Cs selectivity over Rb and K, likely controlled by
408 soils and sedimentary rocks unique to UCC (White, 2013).

409 Almost all the samples (either fresh or altered) show a Cs/Rb ratio of around 0.04 and Cs/K
410 of 0.16 x 10^{-3}, except two partly altered samples (1 and 13) and one almost altered (12 A)
411 (Table 6).

Sample	Cs/Rb	(Cs/ K)(x10^{-3})
2 F	0.04	0.18
4 F	0.04	0.17
6 F	0.03	0.11
11 F	0.03	0.11
1 PA	0.13	0.34
13 PA	0.45	3.01
9 PA	0.04	0.19
8 A	0.05	0.24
10 A	0.06	0.33
12 A	0.06	0.46

412 Table 6. Cs/Rb and Cs/K ratios

In sedimentary rocks illite and/or illite/smectite tend to adsorb Cs and Rb irreversibly in crystallite wedges and frayed edge sites (Wampler *et al*., 2012; Fuller *et al*., 2015). On the other hand, mordenite has been extensively used to remove Cs from water due to its adsorption capacity (Munthali *et al*., 2015, and references therein).. Therefore, it could be interpreted that the anomalies are partially due to an original enrichment of magma coming from the fusion of a crust rich in clay minerals (an active volcanic tectonic environment is proposed in this work) such as Jurassic and Cretaceous thick carbonatic-pelitic sequences widespread in the area (Vaca Muerta, Agrio Formation, etc., Narciso *et al*., 2004) and that, after alteration, new formed minerals could favor the retention of the original anomalies.

During the cooling of rhyolitic viscous lava, anhydrous mineral assemblages would have formed on spherulites (tridymite/cristobalite and potassium feldspar intergrowth). This process could have happened in the volcanic conducts while magma was still hot (Castro *et al*., 2008) and been limited up to ~ 400 °C (Watkins *et al*., 2009). As spherulite growth progressed, the surrounding glass got enriched in water (Castro *et al*., 2008). In addition, concentric and radial fractures formed due to volume changes associated with crystal growth, hydration, and volatile exsolution (von Aulock *et al*., 2013). Once lava flows were extruded, outer surfaces got cooler and more viscous than the center of the flow, producing local high strain rates and subsequent brecciation (McPhie *et al*., 1993). Perlitization must have occurred after spherulite formation (and spherulite-related cracking) at low temperatures (von Aulock *et al*., 2013) and mainly by diffusion of meteoric water in the glass (Denton *et al*., 2009). This process probably continued in glass and welded matrix during and after brecciation, as indicated by petrography (Fig. 4). So the alteration would

435 not be associated with the volcanism that originated the glass but would have occurred after
436 its perlitization and brecciation processes.
437 The fluids involved in the alteration process must have been heated to be able to form the
438 zeolites. The magmatic activity in the area began in the Oligocene, after the start of the
439 uplift of Andean Ranges in the Paleogene, and has continued intermittently, limited by the
440 orogenic phases, until practically the present (Narciso *et al*, 2004). The circulation of fluids
441 caused by the uplift of the Andean Ranges is evidenced by the presence of oil in perlitic
442 cracks. The oil formation in the basin (Agrio Formation) dates between 85 and 30 Ma (Late
443 Cretaceous-Paleogene) (Vergani *et al*., 2011).
444 As mentioned before, the protolith of the mineralization corresponds to rhyolites that
445 discordantly overlie the Upper Cretaceous sediments of the Neuquén Group and are
446 covered by Tertiary basalts (MEC) and Quaternary sediments. Geochemically, they are not
447 comparable with Molle and Puntilla del Huincán basalts and tuff (MEC), or Huincán
448 andesites (HEC), but have similarities with rhyolites from CBVC (Suroga *et al*., 2008).
449 Combina and Nullo (2011) integrate the rocks from CBVC as part of the MEC
450 (geochronologically similar) but no rhyolitic rocks were found in the area to support such
451 assumption. According to Suroga *et al.* (2008), those rocks are geochemically and
452 lithologically different to MEC and correlate with the lower part of the Farellones
453 Formation (Chile), composed of andesitic lavas and breccias, and rhyolites with
454 subordinate volcaniclastic rocks.
455 Based on these previous studies and the data presented in this work, rhyolites of the study
456 area could be correlated with rhyolites of CBVC, corresponding to magmas of high-K calc-
457 alkaline series. According to the stratigraphic position (below MEC), a Lower to Middle

Miocene potential age can be assigned. However, additional geochronological and isotopic analyses are needed in order to establish a more precise correlation with other units. After that, circulating water mainly rich in Ca, Sr, and Mg reached the rhyolite bodies and started their alteration with the formation of low amounts of smectites (promoted by partial leaching of alkalis and a high Mg activity). Part of the alkalis should have remained in the system for zeolite formation. Waters may have been then heated during the volcanic activity that started in the Plio-Pleistocene. Evidence of this volcanism is found in the surrounding area on the Payún Matrú Volcano of early Pleistocene age (Narciso *et al*, 2004). These hot waters produced the main glass alteration event (mordenite deposit), favored by high availability of silica and high permeability of the breccias, while perlitic and spherulitic glasses show restricted alteration because of their lower permeability.

5. CONCLUSIONS

To the west of La Pasarela bridge (on No. 40 National Route), 120 km south of Malargüe (province of Mendoza, Argentina) there is a complex of rhyolitic rocks (high-viscosity lavas) that correspond to magmas of high-K calc-alkaline series. They discordantly overlie the Upper Cretaceous sediments of the Neuquén Group and are covered by Tertiary basalts (MEC) and Quaternary sediments.

They are arranged as subvertical dikes and subhorizontal lava flows composed of vitreous rocks with fibrous, spherulitic and perlitic textures, and are geochemically similar to rhyolites of the CBVC (Lower to Middle Miocene age).

In some sectors, autobreccias were formed, giving the rocks more permeability. These zones were subsequently altered and constitute the main source of the zeolite-rich deposit.

The alteration process started by partial alteration of the glass (in perlitic cracks and inside pumiceous cavities) into fine-grained dioctahedral smectites (beidellite-montmorillonite series). After that, a strong alteration process transformed a great percentage of the glass into mordenite. Later, Ca-clinoptilolite crystallized, mainly inside cavities. Finally, low temperature K-feldspars in veins and open spaces, and at the boundaries of former plagioclase crystals, appeared as the last episode, together with colloform silica.

ACKNOWLEDGEMENTS

Financial support was provided by PICT 2015 Nº 367 (FONCyT). Authors thank CETMIC, CICTERRA (CONICET-UNC), CIC from the province of Buenos Aires and the Geology Department, UNS-CGAMA. Authors also thank Dr. Linda Campbell (University of Manchester, UK) for her recommendations for chemical analyses on zeolites by EPMA. We are very grateful to the editor and reviewers for their comments and recommendations, which have improved the manuscript.

REFERENCES

Barrer, R.M. 1982. Hydrothermal chemistry of zeolites, Academic Press: 360 p. London.

Bengochea, L.; Mas, G.; Maiza, P.; Bengochea, J. 1997. Mordenite occurrence in the Mendoza Province, Argentina. *In* 5th International Conference on the occurrence, properties and utilization of natural zeolites (Zeolite '97): 63-64. Ischia, Italy.

Boynton, W.V. 1984. Cosmochemistry of the rare earth elements: meteorite studies. *In* Developments in Geochemistry, Volume 2: Rare Earth Element Geochemistry (Henderson, P.; editor). Chapter 3, Elsevier: 63-114. Amsterdam.

504 Campbell, L.S.; Charnock, J.; Dyer, A.; Hillier, S.; Chenery, S.; Stoppa, F.; Henderson,
505 C.M.B.; Walcott, R.; Rumsey, M. 2016. Determination of zeolite-group mineral
506 compositions by electron probe microanalysis. Mineralogical Magazine 80 (5): 781-807.
507 Cappelletti, P.; Cerri, G.; de'Gennaro, M.; Langella, A.; Naitza, S.; Padalino, G.; Rizzo, R.;
508 Palomba, M. 2001. Natural zeolites from Cenozoic pyroclastic flows of Sardinis (Italy):
509 evidence of different minerogenetic processes. *In* Proceedings of the 10th International
510 Symposium on Water Rock Interaction.
511 Castro, J.M.; Beck, P.; Tuffen, H; Nichols, A.R.L.; Dingwell, D.B.; Martin, M.C. 2008.
512 Timescales of spherulite crystallization in obsidian inferred from water concentration
513 profiles. American Mineralogist 93 (11-12): 1816–1822.
514 Christidis, G. 1998. Comparative study of the mobility of major and trace elements during
515 alteration of an andesite and a rhyolite to bentonite, in the Islands of Milos and Kimolos,
516 Aegean, Greece. Clays and Clay Minerals 46 (4): 379-399.
517 Christidis, G. 2001. Formation and growth of smectites in bentonites: a case study from
518 Kimolos Island, Aegean, Greece. Clays and Clay Minerals 49 (3): 204-215.
519 Combina, A.M.; Nullo, F. 2011. Ciclos tectónicos, volcánicos y sedimentarios del
520 Cenozoico del sur de Mendoza – Argentina (35º-37ºS y 69º30'W). Andean Geology 38 (1):
521 198-218.
522 Demina, Y.; Frolova, J.; Rychagov, S. 2015. Hydrothermal alterations and petrophysical
523 properties: A case study of Yagodninskoe zeolite deposit, Kamchatka peninsula. *In*
524 Proceedings of the World Geothermal Congress: 1-7. Melbourne, Australia.
525 Denton, J.S.; Tuffen, H.; Gilbert, J.S.; Odling, N. 2009. The hydration and alteration of
526 perlite and rhyolite. Journal of the Geological Society 166 (5): 895-904.

527 Ellis, A.J. 1960. Mordenite synthesis in a natural hydrothermal solution. Geochimica et
528 Cosmochimica Acta 19 (2): 145-146.
529 Fuller, A.J., Shaw, S., Ward, M.B., Haigh, S.J., Mosselmans, J.F.W., Peacock, C.L.,
530 Stackhouse, S.,bDent, A.J., Trivedi, D., and Burke, I.T., 2015, Caesium incorporation and
531 retention in illite interlayers: Applied Clay Science, v. 108, p. 128–134
532 Gargiulo, M.F.; Crosta, S.; Leal, P.R.; Vattuone, M.E. 2017. Las zeolitas naturales de
533 Argentina. *In* Las zeolitas naturales de Iberoamérica (Costafreda Mustelier, J.L.; Martín
534 Sánchez, D.A.; Costafreda Velázquez, J.L.; editors). Fundación Gómez Pardo: 58-136.
535 Madrid.
536 Ghiara, M.R.; Petti, C.; Franco, E.; Lonis, R.; Luxoro, S.; Gnazzo, L. 1999. Occurrence of
537 clinoptilolite and mordenite in Tertiary calc-alkaline pyroclastites from Sardinia (Italy).
538 Clays and Clay Minerals 47 (3): 319-328.
539 Gottardi, G.; Galli, E. 1985. Natural Zeolites. Springer-Verlag: 409 p. Berlin.
540 Grant, J.A. 1986. The isocon diagram, a simple solution to Gresens' equation for
541 metasomatic alteration. Economic Geology 81 (8): 1976-1982.
542 Grant, J.A. 2005. Isocon analysis: A brief review of the method and applications. Physics
543 and Chemistry of the Earth 30 (17-18): 997-1004.
544 Guo, S., Ye, K., Chen, Y., Liu, J.B. 2009. A normalization solution to mass transfer
545 illustration of multiple progressively altered samples using the isocon diagram. Economic
546 Geology 104 (6): 881-886.
547 Hay, R.L. 1977. Geology of zeolites in sedimentary rocks. *In* Mineralogy and Geology of
548 Natural Zeolites (Mumpton, F.A.; editor). Reviews in Mineralogy 4, Mineralogical Society
549 of America: 53-64. Washington.

Hay, R.L.; Sheppard, R.A. 1977. Zeolites in open hydrologic systems. *In* Mineralogy and Geology of Natural Zeolites (Mumpton, F.A.; editor). Reviews in Mineralogy 4, Mineralogical Society of America: 63-102. Washington.

Hawkins, D.B.; Sheppard, R.A.; Gude, A.J. 1978. Hydrothermal synthesis of clinoptilolite and comments on the assemblage phillipsite-clinoptilolite-mordenite. *In* Natural Zeolites: Occurrence, Properties, Use (Sands, L.B.; Mumpton, F.A., editors). Pergamon Press: 337-343. New York.

Hess, P.C. 1966. Phase equilibria of some minerals in the K_2O-Na_2O-Al_2O_3-SiO_2-H_2O system at 25°C and 1 atmosphere. American Journal of Science 264: 289-309.

Irvine, T.N.; Baragar, W.R.A. 1971. A guide to the chemical classification of the common volcanic rocks. Canadian Journal of Earth Sciences 8 (5): 523-548.

Kirov, G.N.; Pechigargov, V.; Landzheva, E. 1979. Experimental crystallization of volcanic glasses in a thermal gradient field. Chemical Geology 26 (1-2): 17-28.

Kitsopoulos, K.P. 1997. The genesis of a mordenite deposit by hydrothermal alteration of pyroclastics on Polyegos Island, Greece. Clay and Clay Minerals 45 (5): 632-648.

Llambías, E.J.; Bertotto, G.W.; Risso, G.; Hernando, I. 2010. El volcanismo cuaternario en el retroarco de Payenia: una revisión. Revista de la Asociación Geológica Argentina 67 (2): 278-300.

Le Bas, M.J.; Le Maitre, R.W.; Streckeisen, A.; Zanettin, B. 1986. A chemical classification of volcanic rocks based on the total alkali–silica diagram. Journal of Petrology 27 (3): 745-750.

McLennan, S.M., 2001. Relationships between the trace element composition of sedimentary rocks and upper continental crust. Geochemistry Geophysics Geosystems, v. 2, 1021, doi: 10 .1029 /2000GC000109.

Marantos, I.; Christidis, G.; Ulmanu, M. 2012. Zeolite formation and deposits. *In* Handbook of Natural Zeolites (Inglezakis, V.J. and Zorpas, A.A.; editors). Bentham Science Publisher: 28-51. USA.

Mariner, R.H.; Surdam, R.C. 1970. Alkalinity and formation of zeolites in saline alkaline lakes. Science 170 (3961): 977-980.

May, V.R.; Chivas, A.R.; Dosseto, A.; Honda, M.; Matchan, E.L.; Phillips, D.; Price, D.M. 2018. Quaternary volcanic evolution in the continental back-arc of southern Mendoza, Argentina. Journal of South American Earth Sciences 84: 88-103.

McPhie, J.; Doyle, M.; Allen, R. 1993. Volcanic Textures: a Guide to the Interpretation of Textures in Volcanic Rocks. Centre for Ore Deposit and Exploration Studies, University of Tasmania: 198 p. Hobart.Meunier, A. 2005. Clays. Springer-Verlag: 472 p. Berlin.

Mormone, A.; Ghiara, M.R.; Balassone, G.; Piochi, M.; Lonis, R.; Rossi, R. 2018. High-silica zeolites in pyroclastic flows from Central Sardinia (Italy): clues on genetic processes and reserves from a mineralogical study. Mineralogy and Petrology 112 (6):767-788.

Munthali, M.W.; Johan, E.; Aono, H.; Matsue, N. 2015. Cs^{+} and Sr^{2+} adsorption selectivity of zeolites in relation to radioactive decontamination. Journal of Asian Ceramic Societies 3 (3): 245-250.

Narciso, V.; Zanettini, J.; Santamaría, G.; Leanza, H. 2004. Hoja geológica 3769-I. Barrancas. Provincias de Mendoza y Neuquén. Boletín 253, SEGEMAR: 60 p. Buenos Aires.

Nullo, F.E.; Stephens, G.C.; Otamendi, J.; Baldauf, P.E. 2002. El volcanismo del Terciario Superior del sur de Mendoza. Revista de la Asociación Geológica Argentina 57 (2): 119-132.

Passaglia, E.; Sheppard, R. 2001. The crystal chemistry of zeolites. *In* Natural Zeolites: Occurrence, Properties, Applications (Bish, D.L.; Ming, D.W.; editors). Reviews in Mineralogy and Geochemistry 45, Mineralogical Society of America: 69-115. Chantilly.

Pearce, J.A.; Harris, N.B.W.; Tindle, A.G. 1984. Trace element discrimination diagrams for the tectonic interpretation of granitic rocks. Journal of Petrology 25 (4): 956-983.

Peccerillo, A.; Taylor, S.R. 1976. Geochemistry of Eocene calc-alkaline volcanic rocks from the Kastamonu Area, Northern Turkey. Contribution to Mineralogy and Petrology 58: 63-81.

Phillips, L.V. 1983. Mordenite occurrences in the Marysvale area, Piute County, Utah: A field and experimental study. Brighman Young University Geology Studies 30 (1): 95-111.

Seki, Y. 1973. Ionic substitution and stability of mordenite. Journal of the Geological Society of Japan 79 (10): 669-676.

Senderov, E.E. 1963. Crystallization of mordenite under hydrothermal conditions. Geochemistry 9: 848-859.

Senkayi, A.L.; Dixon, J.B.; Hossner, L.R.; Abder-Ruhman, M.; Fanning, D.S. 1984. Mineralogy and genetic relationships of Tonstein, bentonite, and lignitic strata in the Eocene Yegua Formation of East-Central Texas. Clays and Clay Minerals 32 (4): 259-271.

Sheppard, R.A.; Gude, A.J.; Fitzpatrick, J.J. 1988. Distribution, characterization, and genesis of mordenite in Miocene tuffs at Yucca Mountain, Nye County, Nevada. U.S. Geol. Surv, Bull. 1777: 1-22.

Sruoga, P.; Rubistein, N.; Etcheverría, M.; Cegarra, M.; Kay, S.; Singer, B.; Lee J. 2008. Estadio inicial del arco volcánico Neógeno en la Cordillera Principal de Mendoza (35ºS). Revista de la Asociación Geológica Argentina 63 (3): 454-459.

Tsolis-Katagas, P; Katagas, C. 1990. Zeolitic diagenesis of Oligocene pyroclastic rocks of the Metaxades area, Thrace, Greece. Mineralogical Magazine 54: 95-103.

Vergani, G.; Arregui, C.; Carbone, O. 2011. Sistemas petroleros y tipos de entrampamientos en la Cuenca Neuquina. *In* XVIII Congreso Geológico Argentino: 645-656. Neuquén, Argentina.

von Aulock, F.W.; Nichols, A.R.L.; Kennedy, B.M.; Oze, C. 2013. Timescales of texture development in a cooling lava dome. Geochimica et Cosmochimica Acta 114: 72-80.

Wampler, J.M., Krogstad, E.J., Elliott, W.C., Kahn, B., and Kaplan, D.I., 2012, Long-term selective retention of natural Cs and Rb by highly weathered coastal plain soils: Environmental Science & Technology, v. 46, p. 3837–3843, doi: 10 .1021 /es2035834.

Watkins, J.; Manga, M.; Huber, C.; Martin, M. 2009. Diffusion-controlled spherulite growth in obsidian inferred from H2O concentration profiles. Contribution to Mineralogy and Petrology 157 (2): 163-172.

White, W.M., 2013, Geochemistry of the solid Earth: The crust. *In* White, W.M. Geochemistry. Wiley-Blackwell; editor, p. 529–557.

Whitney, D.L.; Evans, B.W. 2010. Abbreviations for names of rock-forming minerals. American Mineralogist 95: 185-187.

Wirsching, U. 1976. Experiments on hydrothermal alteration processes of rhyolitic glass in closed and "open" system. Neues Jahrbuch der Mineralogie Monalhejte 5: 203-213.

Highlights

A rhyolitic complex from the province of Mendoza (Argentina) is studied.

Zones of high permeability in autobreccias host a mordenite-rich deposit .

Associated phases comprise clinoptilolite, smectites, K-feldspars and colloform silica.

Host rocks correspond to rhyolitic magmas of high-K calc-alkaline series.

Rhyolites overlie Upper Cretaceous sediments and are covered by Cenozoic deposits.

A correlation with rhyolites of Cordón del Burrero Volcanic Complex is proposed.

Declaration of competing interest

The authors declare that they have no known competing financial interests or personal relationships that could have appeared to influence the work reported in this paper.